

Excitations of a Bose-condensed gas in anisotropic traps

D. A. W. Hutchinson and E. Zaremba

Department of Physics, Queen's University, Kingston, Ontario, Canada K7L 3N6
(November 11, 2018)

We investigate the zero-temperature collective excitations of a Bose-condensed atomic gas in anisotropic parabolic traps. The condensate density is determined by solving the Gross-Pitaevskii (GP) equation using a spherical harmonic expansion. The GP eigenfunctions are then used to solve the Bogoliubov equations to obtain the collective excitation frequencies and mode densities. The frequencies of the various modes, classified by their parity and the axial angular momentum quantum number, m , are mapped out as a function of the axial anisotropy. Specific emphasis is placed upon the evolution of these modes from the modes in the limit of an isotropic trap.

I. INTRODUCTION

The observation [1–3] of the collective modes of the Bose condensate in ultracold trapped atomic gases has stimulated a number of calculations of the collective excitations in these systems. Most of these calculations have been performed using the standard Bogoliubov equations for $T = 0$ [4–11], assuming all the atoms to be in the condensate, although some finite-temperature calculations [12,13], which make use of the Hartree-Fock-Bogoliubov equations within the Popov approximation, have also appeared. Both approaches have been used to investigate the excitations in model isotropic traps, and in anisotropic traps typically corresponding to the experimental trap of the JILA group [1].

At the level of the Bogoliubov approximation, the collective excitations are determined equivalently by solving the coupled Bogoliubov equations, the linearized time-dependent Gross-Pitaevskii (GP) equation or a pair of hydrodynamic-like equations for the condensate density and velocity field. The methods of solution have included analytical solutions within the Thomas-Fermi approximation for the condensate [4,14,15], variational solutions of the time-dependent GP equation [8,9] and expansion techniques for the solution of the Bogoliubov equations using harmonic oscillator bases [5,10]. In this paper we develop an alternative method of solution for arbitrary anisotropic traps which is based on the construction of the GP equation eigenstates in terms of a spherical harmonic expansion. The expansion of the Bogoliubov quasiparticle amplitudes in terms of these functions then leads to a simplified eigenvalue problem which is used to map the collective excitation spectrum throughout much of the anisotropy parameter space. In addition, by analyzing the mode densities, we are able to provide a more detailed discussion than previously available of the evolution of the modes from the isotropic limit.

II. THEORY

The ground state properties of a trapped atomic Bose gas are well-represented by the stationary GP equation

$$\left[-\frac{\hbar^2 \nabla^2}{2m} + V_{ext}(\mathbf{r}) + gn_c(\mathbf{r}) \right] \Phi_0(\mathbf{r}) = \mu \Phi_0(\mathbf{r}), \quad (1)$$

where $n_c(\mathbf{r}) \equiv |\Phi_0(\mathbf{r})|^2$ is the condensate density normalized to the total number of particles N . $V_{ext}(\mathbf{r})$ is the external confining potential and $g = 4\pi\hbar^2 a/m$ is the interaction strength determined by the s -wave scattering length a . The ground state eigenvalue μ is identified with the chemical potential of the condensate. In the following, we assume that $V_{ext}(\mathbf{r})$ is axially symmetric, $V_{ext}(\mathbf{r}) = V_{ext}(r, \theta)$, in which case $\Phi_0(\mathbf{r}) = \Phi_0(r, \theta)$.

Our approach to the solution of the Bogoliubov equations is a basis-set expansion method which makes use of the eigenfunctions of the ground state GP Hamiltonian. These solutions can be chosen to be eigenfunctions of L_z with an angular dependence of $e^{im\phi}$, where m is an integer. To construct these solutions, we convert (1) to a matrix problem by making use of a set of normalized basis functions $\psi_{nlm}(\mathbf{r}) = R_{nl}(r)Y_{lm}(\hat{\mathbf{r}})$ which are the eigenfunctions of the Hamiltonian $\hat{h}_0 = -\frac{\hbar^2 \nabla^2}{2m} + V_0(r)$, where $V_0(r)$ is some spherically symmetric potential. One possible choice for this potential is the spherical average of the external potential which we assume to be of the harmonic form

$$V_{ext}(r, \theta) = \frac{1}{2}m\omega_r^2(x^2 + y^2) + \frac{1}{2}m\omega_a^2z^2. \quad (2)$$

Here, ω_r and ω_a are the radial and axial harmonic frequencies, respectively. We now expand the external potential in terms of Legendre polynomials

$$V_{ext}(r, \theta) = \sum_l V_{ext}^{(l)}(r) P_l(\cos \theta), \quad (3)$$

where

$$V_{ext}^{(l)}(r) = \frac{2l+1}{2} \int_0^\pi d\theta \sin \theta P_l(\cos \theta) V_{ext}(r, \theta). \quad (4)$$

The $l = 0$ component is the spherical average $V_{ext}^{(0)}(r) = \frac{1}{2}mr^2\bar{\omega}^2$, where $\bar{\omega}^2 = \frac{1}{3}(2\omega_r^2 + \omega_a^2)$ is the arithmetic mean of the squares of the axial and radial frequencies. The only other term in the expansion of the external potential is the $l = 2$ component $V_{ext}^{(2)}(r) = \frac{1}{2}mr^2\beta\bar{\omega}^2$ where

$$\beta = \frac{2\omega_a^2 - 2\omega_r^2}{2\omega_r^2 + \omega_a^2} \quad (5)$$

defines the anisotropy parameter. It varies over the range $-1 \leq \beta \leq 2$, where $\beta = -1$ corresponds to the infinitely long cigar-shaped trap and $\beta = 2$ the infinitesimally thin pancake-shaped trap. The JILA trap [1] has $\beta = 1.40$ while the MIT trap [2] has $\beta = -0.991$.

Alternatively, we could use the $l = 0$ component of the total effective potential $V(\mathbf{r}) \equiv V_{ext}(\mathbf{r}) + gn_c(\mathbf{r})$ appearing in (1). Regardless of the choice, we define $V(\mathbf{r}) = V_0(r) + \Delta V(\mathbf{r})$ where $\Delta V(\mathbf{r})$ is the nonspherical perturbation. (Depending on the choice of $V_0(r)$, $\Delta V(\mathbf{r})$ may in fact include an $l = 0$ component.) Expanding an arbitrary solution of (1) as $\phi(\mathbf{r}) = \sum_{nlm} a_{nlm} \psi_{nlm}(\mathbf{r})$, the expansion coefficients are determined by the matrix equation

$$(\varepsilon_{nl} - \varepsilon)a_{nlm} + \sum_{n'l'm'} \langle nlm | \Delta V | n'l'm' \rangle a_{n'l'm'} = 0, \quad (6)$$

where ε is a possible eigenvalue and ε_{nl} are the eigenvalues of \hat{h}_0 . For an axially symmetric potential,

$$\langle nlm | \Delta V | n'l'm' \rangle = \langle nlm | \Delta V | n'l'm \rangle \delta_{mm'} \quad (7)$$

so that states with different m -values remain uncoupled. However the nonspherical perturbation does have the effect of coupling basis states with different l -values. An explicit expression for the potential matrix element is

$$\langle nlm | \Delta V | n'l'm \rangle = \sum_{\bar{l}} A_{\bar{l}ll'}^m \int_0^\infty dr r^2 R_{nl}(r) R_{n'l'}(r) \Delta V_{\bar{l}}(r) \quad (8)$$

where $\Delta V_{\bar{l}}(r)$ are the angular components of $\Delta V(\mathbf{r})$ defined in analogy with those of $V_{ext}(\mathbf{r})$. The numerical coefficient in (8) is

$$A_{\bar{l}ll'}^m = \sqrt{\frac{2l' + 1}{2l + 1}} \langle \bar{l}l'00 | l0 \rangle \langle \bar{l}l'0m | lm \rangle \quad (9)$$

where $\langle l_1 l_2 m_1 m_2 | l_3 m_3 \rangle$ is the usual Clebsch-Gordon coefficient [16]. If ΔV has reflection symmetry in the $x-y$ plane as assumed, only states of the same parity are coupled (l and l' both even or both odd). This restriction implies that the different m -states can be chosen to have a well-defined parity $\Pi = (-1)^{l+m}$ with respect to reflections in the $x-y$ plane.

The condensate wave function, $\Phi_0(\mathbf{r}) = \sqrt{N}\phi_0(\mathbf{r})$, is determined by the lowest energy even-parity solution of (6) in the $m = 0$ subspace and is given by

$$\Phi_0(r, \theta) = \sqrt{N} \sum_{nl} a_{nl0}^{(0)} R_{nl}(r) Y_{l0}(\mathbf{r}). \quad (10)$$

We can now evaluate the condensate density $n_c(r, \theta)$, which has an expansion similar to that of the potential:

$$n_c(r, \theta) = \sum_l n_l(r) P_l(\cos \theta). \quad (11)$$

Comparing (11) to the square of (10), we obtain

$$n_{\bar{l}}(r) = \frac{N}{4\pi} \sum_{\substack{n'l \\ n'l'}} \sqrt{(2l+1)(2l'+1)} |\langle ll'00|\bar{l}0\rangle|^2 a_{nl0}^{(0)} a_{n'l'0}^{(0)} R_{nl}(r) R_{n'l'}(r). \quad (12)$$

These radial functions provide what is needed to complete the specification of the nonspherical potential ΔV . Since Eq.(6) depends on the condensate density through ΔV , this equation must be iterated until a self-consistent solution for the condensate wave function is generated.

We determine the collective excitations of the condensate using the Bogoliubov equations, which are equivalent to solving the linearized time-dependent GP equation. As shown in Ref. [12], the Bogoliubov equations can be cast into the form

$$\begin{aligned} \hat{h}^2 \psi_i^{(-)}(\mathbf{r}) + 2g\hat{h}n_c(\mathbf{r})\psi_i^{(-)}(\mathbf{r}) &= E_i^2 \psi_i^{(-)}(\mathbf{r}) \\ \hat{h}^2 \psi_i^{(+)}(\mathbf{r}) + 2gn_c(\mathbf{r})\hat{h}\psi_i^{(+)}(\mathbf{r}) &= E_i^2 \psi_i^{(+)}(\mathbf{r}), \end{aligned} \quad (13)$$

where the functions $\psi_i^{(\pm)}$ are related to the quasiparticle amplitudes by $\psi_i^{(\pm)}(\mathbf{r}) \equiv u_i(\mathbf{r}) \pm v_i(\mathbf{r})$. The Hamiltonian \hat{h} appearing in these equations is the ground state condensate Hamiltonian shifted by the ground state eigenvalue μ . Since these equations are uncoupled, either can be used to determine the excitation energies E_i .

To solve (13) for $\psi_i^{(+)}(\mathbf{r})$ we proceed as in Ref. [12] and introduce the expansion $\psi_i^{(+)}(\mathbf{r}) = \sum_{\alpha} c_{\alpha}^{(i)} \phi_{\alpha}(\mathbf{r})$ where the $\phi_{\alpha}(\mathbf{r})$ are the eigenfunctions of \hat{h} determined from (6), and the expansion coefficients $c_{\alpha}^{(i)}$ are required to be normalized as $\sum_{\alpha} \varepsilon_{\alpha} c_{\alpha}^{(i)*} c_{\alpha}^{(j)} = E_i \delta_{ij}$. Substituting this expansion into the equation for $\psi_i^{(+)}(\mathbf{r})$, we obtain

$$\sum_{\beta} \{M_{\alpha\beta} + \varepsilon_{\alpha} \delta_{\alpha\beta}\} \varepsilon_{\beta} c_{\beta}^{(i)} = E_i^2 c_{\alpha}^{(i)}. \quad (14)$$

Within a particular m -subspace, the matrix $M_{\alpha\beta}$ is given by

$$\begin{aligned} M_{\alpha\beta} &= 2g \int d\mathbf{r} \phi_{\alpha}^{*}(\mathbf{r}) n_c(\mathbf{r}) \phi_{\beta}(\mathbf{r}) \\ &= \sum_{nl'n'l'} a_{nl}^{(\alpha)*} a_{n'l'}^{(\beta)} \langle nlm | 2gn_c | n'l'm \rangle \end{aligned} \quad (15)$$

where $a_{nl}^{(\alpha)}$ is the α -th eigenvector of Eq.(6). Since the matrix $M_{\alpha\beta}$ is diagonal in both the azimuthal quantum number m and the parity Π , these quantum numbers also serve to classify the collective modes. Once the eigenvector $c_{\alpha}^{(i)}$ has been determined, the density of the i -th mode is given by

$$\delta n_i(\mathbf{r}) \propto \phi_0(\mathbf{r}) \psi_i^{(-)}(\mathbf{r}) = \phi_0(\mathbf{r}) \sum_{\alpha} \frac{\varepsilon_{\alpha}}{E_i} c_{\alpha}^{(i)} \phi_{\alpha}(\mathbf{r}). \quad (16)$$

III. RESULTS

As an illustration of the technique we consider the case of 2000 rubidium atoms contained within an axially symmetric harmonic trap of varying anisotropy. For the JILA trap, $\omega_r/2\pi = 75$ Hz and $\omega_a/2\pi = 212$ Hz, giving an anisotropy parameter of $\beta = 1.40$, and an averaged harmonic frequency of $\bar{\omega}/2\pi = 137$ Hz. We keep the latter fixed in our calculations and vary the parameter β . To complete the parameter specification, we take $m(^{87}\text{Rb}) = 1.44 \times 10^{-25}$ kg for the mass of the atoms, and an s -wave scattering length of $a \simeq 110a_0 = 5.82 \times 10^{-9}$ m. Throughout, lengths and energies are expressed in terms of the characteristic oscillator length of the isotropic trap $d = (\hbar/m\bar{\omega})^{1/2} = 9.21 \times 10^{-7}$ m and the characteristic trap energy $\hbar\bar{\omega} = 9.03 \times 10^{-32}$ J, respectively. When expressed in these units, the dimensionless condensate wave function depends only on the dimensionless parameters β and $\gamma \equiv Na/d$.

In Fig. 1 we show the excitation spectrum obtained from the solution of (14). In these calculations the basis functions, generated numerically, are limited in number to between 100 and 200, the actual number being controlled by the value of the high-energy cutoff set in the basis function expansion. This number provided sufficient accuracy over the range of the anisotropy parameter shown. However as β increases towards its extreme values of -1 and 2 , increasingly more basis functions are required to obtain accurate results and our calculations are necessarily curtailed.

The modes shown here are those corresponding to axial quantum numbers $m = 0 - 4$ for both even and odd parity. The modes of even parity are shown in Fig. 1(a) and those of odd parity in Fig. 1(b). Let us first examine the modes of the isotropic trap along the line $\beta = 0$ studied previously [6,12]. In order of increasing frequency, we find a doubly degenerate mode corresponding to the $l = 1$ excitations, followed by the triply degenerate $l = 2$ mode, the quadruply degenerate $l = 3$ mode and a nondegenerate $l = 0$ mode. (In this description, we do *not* include the additional degeneracy associated with the sign of m which is not lifted by axial anisotropy.) It is on the evolution of these modes that we concentrate in the following.

The lowest doubly degenerate $l = 1$ modes for the spherical trap correspond to the centre of mass modes of the harmonic potential [17]. At $\beta = 0$ both modes have a frequency of exactly 1 in units of $\bar{\omega}$. Of these two modes one is the odd parity, $m = 0$ mode, while the other is the even parity $m = 1$ mode. (Recall that parity refers to the reflection symmetry in the x - y plane.) Both of these modes correspond to a rigid oscillation of the condensate density in the axial and transverse directions, respectively. As β begins to deviate from zero, the degeneracy of these two modes is lifted, one oscillating at the frequency ω_a (odd parity) and the other at ω_r (even parity). When expressed in units of $\bar{\omega}$, these modes disperse according to $\omega_a/\bar{\omega} = \sqrt{1+\beta}$ and $\omega_r/\bar{\omega} = \sqrt{1-\beta/2}$. We have plotted these exact results for the center of mass modes in Fig. 1 to illustrate the accuracy of our numerical calculations. Any deviation of the numerical results from the exact values would indicate the need to increase the number of basis functions in the expansions.

For the experiments in the regime where the axial confining potential is stronger than in the radial direction (such as for the JILA trap), the collective modes of interest, other than the centre of mass modes, are those originating from the $l = 2$ mode in the isotropic limit. In particular, the modes observed experimentally [1] are the $m = 0$ and $m = 2$ even parity modes originating from the $l = 2$ mode, the lower frequency mode being the $m = 2$. This latter mode has quadrupolar character, with a density fluctuation which is concentrated in the x - y plane. As a result, the oscillation is mainly influenced by the radial trap frequency ω_r and the mode frequency decreases monotonically with increasing β , similar to the behaviour of the $m = 1$ centre of mass mode. In fact, as will be explained in more detail shortly, these particular $m = 1$ and $m = 2$ modes are the first two members of a family of modes identified by the number ‘1’ in Fig. 1(a).

We now examine the even parity $m = 0$ mode originating from $l = 2$ in more detail. The mode density defined by (16) is shown in Figs. 2 and 3 for a variety of β values. Since the mode density is of the form $\delta n(\mathbf{r}) \propto f(r, \theta)$, the interesting spatial dependence is revealed by considering a plane (e.g. the x - z plane) containing the axis of the trap. Fig. 2 gives the behaviour of the density along the x and z directions while Fig. 3 gives a contour representation. In the isotropic limit, this mode corresponds to the quadrupole $l = 2, m = 0$ mode for which an expansion (contraction) in the radial direction is accompanied by a contraction (expansion) in the axial direction, as shown in the $\beta = 0$ panel of Fig. 2. The contour representation in Fig. 3(b) shows nodal lines making angles of $\pm 54.7^\circ$ with respect to the z -axis. This representation is particularly useful since it indicates the direction of particle flow. In the Thomas-Fermi approximation [4], the velocity field is given by $m \frac{\partial \mathbf{v}}{\partial t} = -g \nabla \delta n$ which implies that the direction of particle flow is normal to the density contours. Although not exact, this relationship between velocity and mode density is still a good guide in the Bogoliubov approximation. Fig. 3(b) thus indicates that for this mode there is a circumferential flow from the equatorial x - y plane to the polar regions.

However, as the magnitude of β is increased from zero, the character of the mode changes from quadrupolar to one which is more accurately described as ‘breathing-like’. For negative β , the cloud breathes in the axial direction, while for positive β , it breathes in the radial direction. Thus, in Fig. 3(a) for $\beta = -0.5$, we see nodal surfaces which are approximately planes perpendicular to the z -axis, indicating a flow of atoms in the axial direction. This mode is analogous to the lowest standing wave resonance in an open-ended organ pipe of length L , with wavelength $\lambda \simeq L$. Conversely, for $\beta = 1.4$ in Fig. 3(c), we see a cylindrical nodal surface and a flow which is predominantly radial. In view of this behaviour, the mode frequency would be expected to depend mainly upon ω_a for negative β and upon ω_r for positive β , resulting in a dispersion to zero in the $\beta \rightarrow -1$ and $\beta \rightarrow 2$ limits. This is precisely the behaviour exhibited by this mode which is the lowest mode labeled ‘3’ in Fig. 1(a). Similar arguments can be used to understand the dispersion of the higher frequency modes once a contour representation of the mode density is available. For example, we show in Figs. 4(a-c) the contour representation of the lowest odd-parity mode labeled ‘4’ in Fig. 1(b), which originates from the $l = 3, m = 0$ mode in the isotropic limit. Fig. 4(a) for $\beta = -0.5$ is clearly the next standing-wave resonance following the fundamental mode illustrated in Fig. 3(a). Likewise, Fig. 4(c) for $\beta = 1.4$ illustrates a hybrid mode which involves both the radial breathing motion of Fig. 3(c) and an oscillation in the axial direction. As a result of this axial motion, this mode has a finite limiting frequency for $\beta \rightarrow 2$.

Also of interest within the anisotropy regime of the JILA experiment is the $m = 3$ mode with even parity, originating from the $l = 3$ mode for the isotropic case (the third curve from the bottom, labeled ‘1’ in Fig. 1(a)). The excitation energy of this mode is only slightly greater than that of the experimentally observed $m = 0$ mode and like the latter, disperses to zero for $\beta \rightarrow 2$. However, as indicated by the common label of ‘1’ in Fig. 1(a), this mode is the third

member of the family mentioned previously, which is distinct from the family labeled ‘3’ that the $m = 0$ mode belongs to. The observability of this $m = 3$ mode would of course depend on the possibility of inducing experimentally an excitation having a $e^{3i\phi}$ azimuthal dependence.

Although the frequency spectrum in Fig. 1 as a function β is quite complex, it is apparent that certain patterns have emerged. These correspond to the families labeled by 1 through 4 in the figure, three of which were alluded to previously. These families correspond to the modes very recently calculated analytically in the Thomas-Fermi limit by Öhberg et al. [14] and independently by Fliesser et al. [15]. (Some of these mode frequencies were obtained earlier by Stringari [4].) Their analytic expressions for the mode frequencies of the four families, converted to our notation, with ω_i corresponding to the i -th group as labeled in Fig. 1, are given below:

$$\begin{aligned}\omega_1^2 &= (1 - \beta/2)m\bar{\omega}^2 \\ \omega_2^2 &= [(1 + \beta) + (1 - \beta/2)m]\bar{\omega}^2 \\ \omega_3^2 &= \left[\frac{3}{2}(1 + \beta) + (m + 1)(2 - \beta) \right. \\ &\quad \left. - 1/2(9(1 + \beta)^2 - 2(m + 4)(2 - \beta)(1 + \beta) + (m + 2)^2(2 - \beta)^2)^{1/2} \right] \bar{\omega}^2 \\ \omega_4^2 &= \left[\frac{7}{2}(1 + \beta) + (m + 1)(2 - \beta) \right. \\ &\quad \left. - 1/2(25(1 + \beta)^2 + 2(m - 4)(2 - \beta)(1 + \beta) + (m + 2)^2(2 - \beta)^2)^{1/2} \right] \bar{\omega}^2.\end{aligned}\quad (17)$$

In the notation of Fliesser et al. [15], these modes are labeled by three quantum numbers (n, j, m) , where m is the usual azimuthal quantum number and n and j are two others which distinguish the radial and angular character of the modes. The four families we have identified correspond to $(0,0,m)$, $(1,0,m)$, $(2,0,m)$ and $(3,0,m)$, respectively. This identification can be checked by considering the limiting values of the analytic result for $\beta \rightarrow -1$ and $\beta \rightarrow 2$, as presented in Table 1. For example, the 1-modes in Fig. 1(a) tend to zero as $\beta \rightarrow 2$ and to a finite value for $\beta \rightarrow -1$, in accord with the analytic results. However the finite limiting values of the numerical results deviate from the analytic value of $\sqrt{3m/2}$, the difference increasing with increasing m (the agreement is exact for the lowest mode in this family since it corresponds to the center of mass mode). The discrepancy between the numerical and analytic results is not due to inaccuracies in the numerical calculations, since we have checked that the numerical basis set is sufficiently large to yield accurate results for the modes shown. Rather, the differences are real and reflect the fact that our calculations are for a finite number of particles, N , while the Thomas-Fermi results correspond to the $N \rightarrow \infty$ limit. Similar deviations appear for the 2-modes in Fig. 1(b). The analytic limits for these modes are $\sqrt{3}$ for $\beta \rightarrow 2$ and $\sqrt{3m/2}$ for $\beta \rightarrow -1$. The lowest 2-mode in Fig. 1(b), the odd-parity center of mass mode, does extrapolate to $\sqrt{3}$ but the higher modes in this family, to within our numerical accuracy, do not. In other words, the finite size of the trapped gas leads to a weak m -dependence of the limiting value, which presumably disappears as $N \rightarrow \infty$. As noted by Fliesser et al. [15], the convergence with N is more rapid for modes having smaller n values, which is consistent with our numerical findings.

Another feature of the mode spectrum worth noting is a number of instances of anticrossing-type behaviour between modes of equal m and the same parity. The most obvious example of this occurs in Fig. 1(a) for the two $m = 0$ modes near $\beta = 1$. Similar behaviour is seen for two of the $m = 0$ odd-parity modes in Fig. 1(b) near $\beta = -0.5$. Of course, there is no avoided crossing of modes with different m values, and there are numerous examples of these crossings in Fig. 1. However for real traps which do not possess ideal cylindrical symmetry, one can expect to see additional anticrossings associated with the coupling between modes induced by trap imperfections.

IV. CONCLUSIONS

In conclusion, we have presented a new and efficient method for solving the Bogoliubov equations for a gas of weakly interacting Bose condensed atoms in an axially symmetric magnetic trap. We have used the method to calculate the low lying collective mode frequencies and densities over a large portion of the anisotropy parameter space. The evolution of the modes as a function of the anisotropy parameter β has provided a more complete understanding of the relationship of the modes in anisotropic traps to those in the isotropic limit. We have also made contact with analytical results obtained in the Thomas-Fermi limit and have identified differences between the

finite- N and infinite- N calculations. We are presently applying our method for anisotropic traps to the problem of finite-temperature excitations in the hydrodynamic regime [18].

ACKNOWLEDGMENTS

This work was supported by grants from the Natural Sciences and Engineering Research Council of Canada.

[1] D. S. Jin, J.R. Ensher, M.R. Matthews, C.E. Weiman and E.A. Cornell, Phys. Rev. Lett. **77**, 420 (1996).
[2] M.-O. Mewes, M.R. Andrew, N.J. van Druten, D.M. Kurn, D.S. Durfee, C.G. Townsend and W. Ketterle, Phys. Rev. Lett. **77**, 988 (1996).
[3] D. S. Jin, M.R. Matthews, J.R. Ensher, C.E. Weiman and E.A. Cornell, Phys. Rev. Lett. **78**, 764 (1997).
[4] S. Stringari, Phys. Rev. Lett. **77**, 2360 (1996).
[5] M. Edwards, P.A. Ruprecht, K. Burnett, R.J. Dodd and C.W. Clark, Phys. Rev. Lett. **77**, 1671 (1996).
[6] K. G. Singh and D. S. Rokhsar, Phys. Rev. Lett. **77**, 1667 (1996).
[7] J. Javanainen, Phys. Rev. A **54**, 3722 (1996).
[8] Y. Castin and R. Dum, Phys. Rev. Lett. **77**, 5315 (1996).
[9] V.M. Pérez-García, H. Michinel, J.I. Cirac, M. Lewenstein and P. Zoller, Phys. Rev. Lett. **77**, 5320 (1996).
[10] L. You, W. Hoston, and M. Lewenstein, Phys. Rev. A **55**, 1581 (1997).
[11] Yu. Kagan, E.L. Surkov and G.V. Shlyapnikov, Phys. Rev. A **55**, R18 (1997).
[12] D.A.W. Hutchinson, E. Zaremba and A. Griffin, Phys. Rev. Lett. **78**, 1842 (1997).
[13] R.J. Dodd, M. Edwards, C.W. Clark and K. Burnett, preprint.
[14] P. Öhberg, E.L. Surkov, I. Tittonen, S. Stenholm, M. Wilkens and G.V. Shlyapnikov, preprint physics/9705006.
[15] M. Fliesser, A. Csordás, P. Szépfalusy and R. Graham, preprint cond-mat/9706002.
[16] A. Messiah, *Quantum Mechanics* (North Holland, Amsterdam, 1966), vol. 2.
[17] See J.F. Dobson, Phys. Rev. Lett. **73**, 2244 (1994) and references therein for a discussion of the center of mass mode in parabolic traps and the generalized Kohn theorem.
[18] E. Zaremba, A. Griffin and T. Nikuni, preprint cond-mat/9705134.

Table 1: Limiting values of the mode frequencies, $\omega_i/\bar{\omega}$, given in Eq.(17).

i	$\beta \rightarrow -1$	$\beta \rightarrow 2$
1	$\sqrt{\frac{3}{2}}m$	0
2	$\sqrt{\frac{3}{2}}m$	$\sqrt{3}$
3	$\sqrt{\frac{3}{2}}m$	0
4	$\sqrt{\frac{3}{2}}m$	$\sqrt{3}$

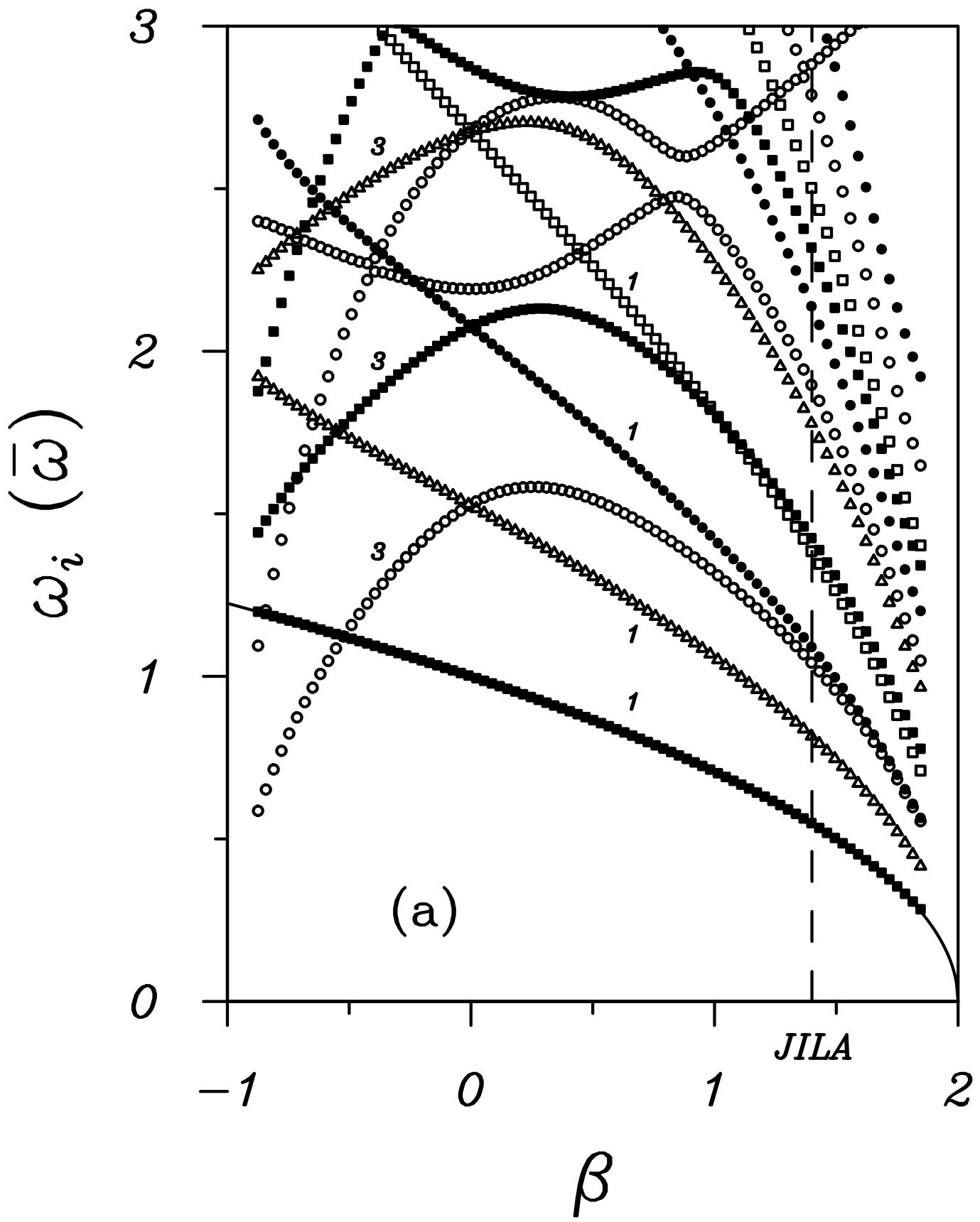
FIGURE CAPTIONS

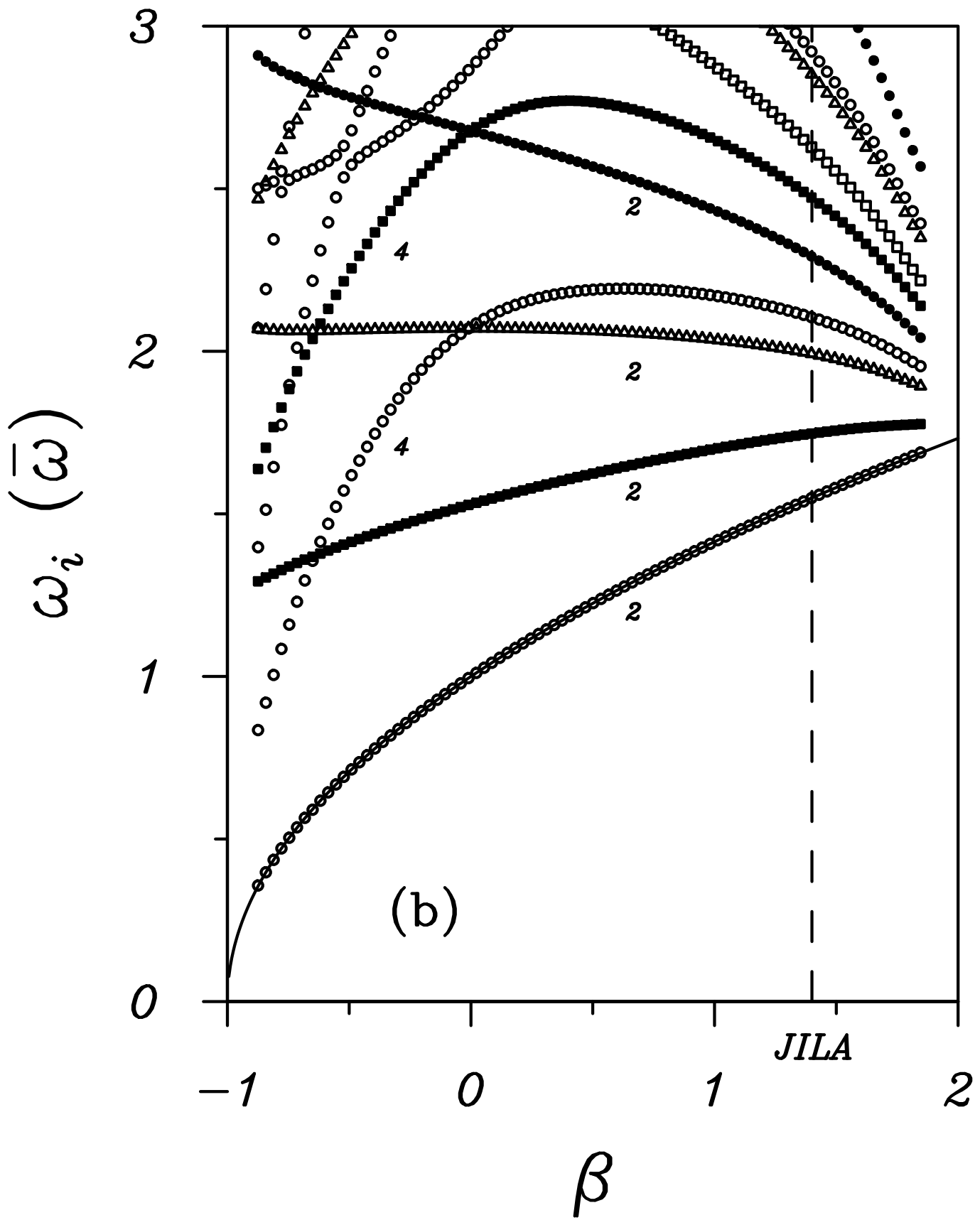
Fig.1: Mode frequencies in units of the average trap frequency $\bar{\omega}$ as a function of the anisotropy parameter β : (a) even-parity modes and (b) odd-parity modes. The symbols code the various m -values: $m = 0$ (open circle), $m = 1$ (filled square), $m = 2$ (open triangle), $m = 3$ (filled circle), $m = 4$ (open square). The numerical labels 1–4 identify the different families of modes as discussed in the text.

Fig.2: Mode density (left panel) and corresponding equilibrium density (right panel) for values of the anisotropy parameter shown. The solid line gives the variation along the x -axis and the chain curve along the z -axis.

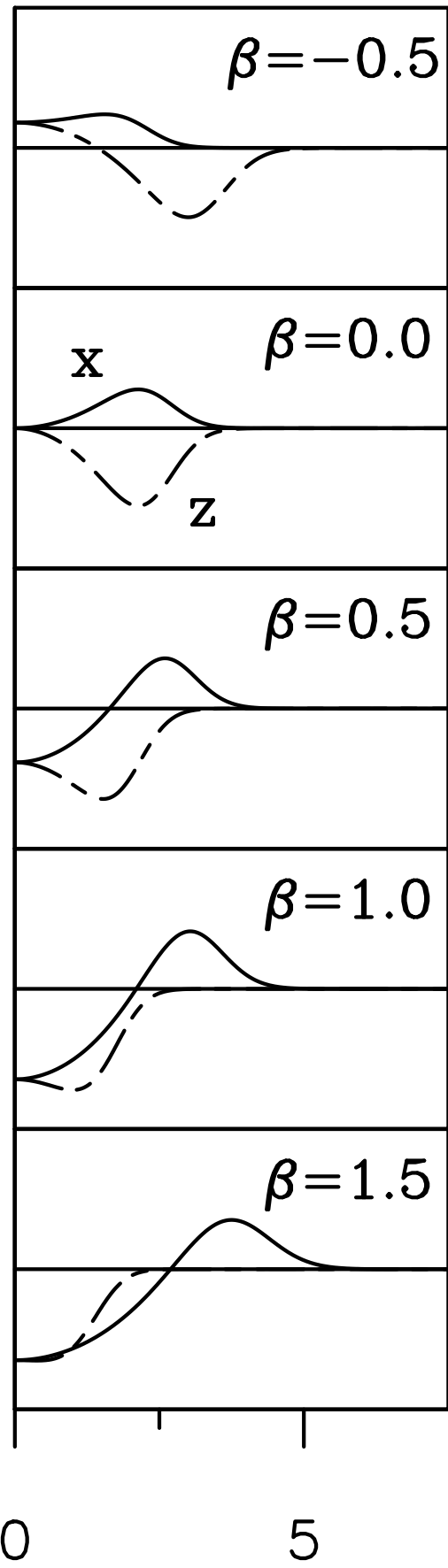
Fig.3: Contour representation of the mode density of the lowest mode ($m = 0$, even parity) labeled ‘3’ in Fig. 1(a): (a) $\beta = -0.5$, (b) $\beta = 0$ and (c) $\beta = 1.4$. The shaded region corresponds to negative values of the mode density, the unshaded region to positive values.

Fig.4: As in Fig. 3, but for the lowest mode ($m = 0$, odd parity) labeled ‘4’ in Fig. 1(b).



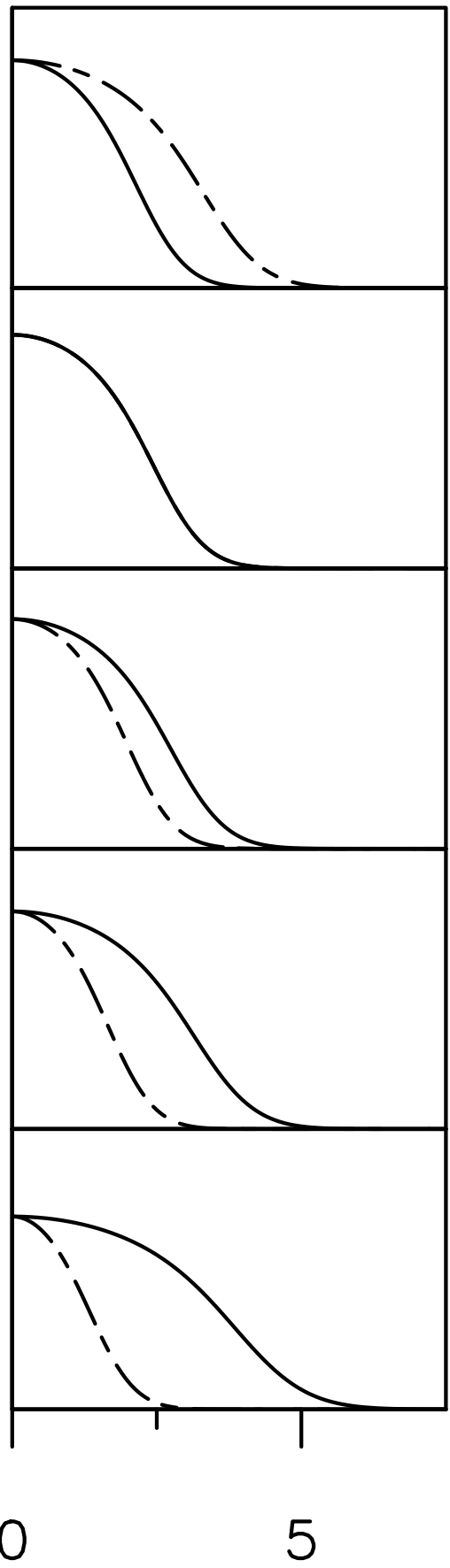


Mode Density (Arb. Units)



$r(d)$

Condensate Wavefunction



$r(d)$

